Bull. Fac. Fish. Hokkaido Univ.
39(3), 167-179. 1988.

# Upwelling Induced by a Cyclonic Storm
## I. Comparison a linear theory with observations

Yoshio AKIBA*

## Abstract

A linear theory of upwelling induced by a cyclonic storm was proposed by the author in 1955. As predicted by this theory, temperature-depth structures observed following hurricane Hilda in the Gulf of Mexico in October of 1964 indicated that warm ocean surface layers were transported outward from the storm center and cold waters upwelled along the storm path.

Similar results were found after typhoon Shirley passed in the vicinity of Kuroshio, Japan in September 1965. The most striking change occured under the eye, where the isotherms rose sharply.

This study was undertaken to compare the original theory and these observations. It was well coincident with observations that intense upwelling was confined to within twice the radius of maximum wind. But steady-state model did not account well for upwelling speed.

## Introduction

Ekman transport with a cyclonic wind system give rise to a divergence of surface water layers and cold water is upwelled at the system center.

In 1955, the author, in collaboration with Hidaka, reported a cold water area after a hurricane passage and proposed a linear theory based upon a stationary cyclonic wind system to explain it. Two observations of ocenographic conditions after the passing of a cyclonic storm have since been carried out by Leipper (1964) and Wright (1965). The stationary study from which the theory was developed has limits in many respects, but the theory explained the observed oceanographic conditions fairly well. A more advanced study is needed to compare the stationary theory and these observations.

### *1. Description of a stationary cyclonic wind system*

A wide homogeneous sea is assumed, and three dimensional cylindrical coordinates in which the $z$ axis is taken vertically downwards. A circular wind is held constant, and the wind stresses do not vary in $\theta$ direction.

Therefore all the vertical and horizontal components of currents can be determined as functions of $r$ and $z$ (Fig. 1).

Rotation of the Earth and frictional forces due to vertical and horizontal mixing are taken into account.

In such a case the hydrodynamical equations are:

* *Laboratory of Oceanography and Meteorology, Faculty of fisheries, Hokkaido University*
(北海道大学水産学部海洋学気象学講座)

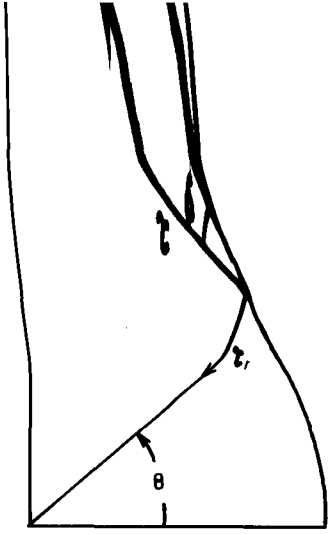


Fig. 1. Tangential and radial components.

$$\begin{aligned}
&\frac{A_v}{\rho}\frac{\partial^2 u}{\partial z^2}+\frac{A_h}{\rho}\left(\frac{\partial^2 u}{\partial r^2}+\frac{1}{r}\frac{\partial u}{\partial r}-\frac{u}{r^2}\right)+2\Omega\sin\phi v-g\frac{\partial\zeta}{\partial r}=0\\
&\frac{A_v}{\rho}\frac{\partial^2 v}{\partial z^2}+\frac{A_h}{\rho}\left(\frac{\partial^2 v}{\partial r^2}+\frac{1}{r}\frac{\partial v}{\partial r}-\frac{v}{r^2}\right)-2\Omega\sin\phi u\qquad=0
\end{aligned}\tag{1}$$

where $A_v$ and $A_h$ are the coefficients of vertical and horizontal mixing of the sea water, $u$ and $v$ the horizontal components of current velocities in the $r$- and $\theta$-directions, $\zeta$ is the surface elevation, $\Omega$ the angular velocity of the earth, $\phi$ the geographic latitude, and $\rho$ the density of the sea water, respectively.

In addition to these, the equation of continuity is:

$$\frac{\partial u}{\partial r}+\frac{u}{r}+\frac{\partial w}{\partial z}=0 \tag{2}$$

since $\partial v/\partial\theta=0$.

The following system is assumed as the distribution of the wind stresses:

$$\begin{aligned}
&\tau=\tau_m\frac{r}{r_m} &&\text{for}\quad 0<r<r_m\\
&\tau=\tau_m\frac{r_m}{r} &&\text{for}\quad r_m<r<\infty
\end{aligned}\tag{3}$$

where $\tau_m$ is the maximum wind stress, $r_m$ is distance from the center of the storm at which $\tau=\tau_m$ (Fig. 2).

On the surface of the sea, the conditions to be satisfied are:

$$\begin{aligned}
-A_v\frac{\partial u}{\partial z}&=\tau_r\\
-A_v\frac{\partial v}{\partial z}&=\tau_\theta
\end{aligned}\tag{4}$$

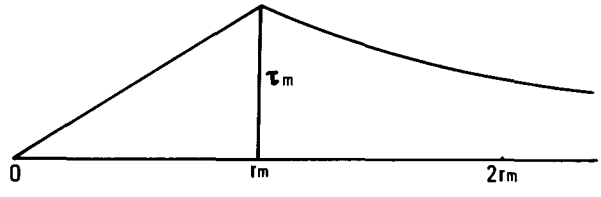


Fig. 2. Distribution of wind stresses.

where $\tau_r$, $\tau_\theta$ are the stress components of the wind in $r$- and $\theta$-directions, considered to be a function of $r$.

At the bottom $z=h$ we must have:

$$u=v=0. \tag{5}$$

Next, the depth of frictional influence and "frictional distance" is introduced as follows:

$$D_v=\pi\sqrt{\frac{A_v}{\rho\Omega\sin\phi}} \quad D_h=\pi\sqrt{\frac{A_h}{\rho\Omega\sin\phi}} \tag{6}$$

Then equation (1) becomes:

$$\begin{aligned} D_v^2\frac{\partial^2 u}{\partial z^2}+\left(\frac{\partial^2}{\partial l^2}+\frac{1}{l^2}\frac{\partial}{\partial l}-\frac{1}{l^2}\right)u-2\pi^2 v-\frac{\pi^2 g}{\Omega\sin\phi D_h}\frac{\partial\zeta}{\partial l}&=0 \\ D_v^2\frac{\partial^2 v}{\partial z^2}+\left(\frac{\partial^2}{\partial l^2}+\frac{1}{l^2}\frac{\partial}{\partial l}-\frac{1}{l^2}\right)v-2\pi^2 u&=0 \end{aligned} \tag{7}$$

where $l=r/D_h$.

In order to solve equations (7), we express $u$, $v$, $\partial\zeta/\partial l$, $\tau$ by the following Bessel-Fourier integrals:

$$\begin{aligned} u&=\int_0^\infty \lambda u_1(z,\lambda)J_1(l\lambda)d\lambda \\ v&=\int_0^\infty \lambda v_1(z,\lambda)J_1(l\lambda)d\lambda \end{aligned} \tag{8}$$

$$\frac{\partial\zeta}{\partial l}=\int_0^\infty \lambda\beta(\lambda)J_1(l\lambda)d\lambda \tag{9}$$

$$\tau=\int_0^\infty \lambda T(\lambda)J_1(l\lambda)d\lambda. \tag{10}$$

Let us introduce $\alpha$ such that:

$$u_1+iv_1=\alpha \tag{11}$$

and substituting equations (8), (9), (10) and (11) into equations (7), the two equations of (7) are combined:

$$D_v^2\frac{d^2\alpha}{dz^2}-(\lambda^2+2\pi i)\alpha-\frac{\pi^2 g\beta}{\Omega\sin\phi D_h}=0 \tag{12}$$

and the boundary conditions to be satisfied become

$$\text{at} \quad z=h \qquad \alpha=0 \tag{13}$$

$$\text{at} \quad z=0 \qquad -A_v\frac{d\alpha}{dz}=T(\lambda) \tag{14}$$

$T(\lambda)$ can be obtained by Hankel-transformation of (10) as follows:

$$T(\lambda)=\int_0^\infty l\tau J_1(\lambda)dl \tag{15}$$

Substituting (3) into (15) we have:

$$T(\lambda)=\frac{2\tau_m J_1(a\lambda)}{\lambda^2} \tag{16}$$

where

$$a=\frac{r_m}{D_h}. \tag{17}$$

When the depth of the sea is sufficient, we have:

$$\beta(\lambda) \longrightarrow 0. \tag{18}$$

The solutions of (7) are shown as:

$$\alpha = \frac{2\tau_m}{\lambda^2\sqrt{\lambda^2+2\pi^2 i}} \cdot J_1(a\lambda) \cdot \exp\left(-\sqrt{\lambda^2+2\pi^2 i}\,\frac{z}{D_v}\right). \tag{19}$$

If we separate the real part $P$ of $\sqrt{\lambda^2+2\pi^2 i}$ from the imaginary $Q$, we have:

$$\begin{aligned} P &= \sqrt{(\sqrt{(\lambda^4+4\pi^2)}+\lambda^2)/2} \\ Q &= \sqrt{(\sqrt{(\lambda^4+4\pi^2)}-\lambda^2)/2}. \end{aligned} \tag{20}$$

Thus horizontal components of velocity are given by:

$$\begin{aligned} u &= \frac{2D_v}{A_v}\tau_{m\theta}K_1 + \frac{2D_v}{A_v}\tau_{ml}K_2 \\ v &= \frac{2D_v}{A_v}\tau_{m\theta}K_2 - \frac{2D_v}{A_v}\tau_{ml}K_1 \end{aligned} \tag{21}$$

where

$$\begin{aligned} K_1 &= \int_0^\infty R(l, \lambda)M(z, \lambda)d\lambda \\ K_2 &= \int_0^\infty R(l, \lambda)N(z, \lambda)d\lambda, \end{aligned} \tag{22}$$

and $R$, $M$, $N$ are

$$R(l, \lambda) = \frac{J_1(a\lambda)J_1(l\lambda)}{\lambda} \tag{23}$$

$$M(z, \lambda) = \exp\left(-P\frac{z}{D_v}\right) \cdot \left\{\frac{P\sin\left(Q\frac{z}{D_v}\right) + Q\cos\left(Q\frac{z}{D_v}\right)}{P^2+Q^2}\right\}$$

$$N(z, \lambda) = \exp\left(-P\frac{z}{D_v}\right) \cdot \left\{\frac{P\cos\left(Q\frac{z}{D_v}\right) - Q\sin\left(Q\frac{z}{D_v}\right)}{P^2+Q^2}\right\} \tag{24}$$

The equation of continuity can be rewritten as:

$$\frac{1}{D_h}\frac{\partial}{\partial l}(ul) + \frac{\partial}{\partial z}(wl) = 0 \tag{25}$$

If we define a function $\Psi$ as

$$ul = -\frac{\partial \Psi}{\partial z}, \quad wl = \frac{1}{D_h} \cdot \frac{\partial \Psi}{\partial l} \tag{26}$$

$\Psi$ is given as

$$\Psi = \frac{2D_v^2}{A_v}\tau_{m\theta}\Psi_\theta + \frac{2D_v^2}{A_v}\tau_{ml}\Psi_l \tag{27}$$

where $\Psi_\theta$, $\Psi_l$ are

$$\begin{aligned} \Psi_\theta &= l\int_0^\infty R(l, \lambda)L_1(z, \lambda)d\lambda \\ \Psi_l &= l\int_0^\infty R(l, \lambda)L_2(z, \lambda)d\lambda, \end{aligned} \tag{28}$$

and $L_1$, $L_2$ are

$$L_1=\frac{1}{(P^2+Q^2)^2}\left\{(P^2-Q^2)\left(\cos\left(Q\frac{z}{D_v}\right)\exp\left(-P\frac{z}{D_v}\right)-1\right)\right.$$
$$\left.-2PQ\exp\left(-P\frac{z}{D_v}\right)\sin\left(Q\frac{z}{D_v}\right)\right\} \tag{29}$$

$$L_2=\frac{1}{(P^2+Q^2)^2}\left\{(P^2-Q^2)\sin\left(Q\frac{z}{D_v}\right)\exp\left(-P\frac{z}{D_v}\right)\right.$$
$$\left.+2PQ\left(\cos\left(Q\frac{z}{D_v}\right)\exp\left(-P\frac{z}{D_v}\right)-1\right)\right\} \tag{30}$$

A function $\Psi$ can be treated as a stream function, $\Psi=$constant indicate stream lines.

The vertical component of velocity is now given by

$$w=\frac{1}{D_h}\cdot\frac{2D_v^2}{A_v}\cdot\tau_{m\theta}\cdot\frac{1}{l}\int_0^\infty R(l,\lambda)L_2(z,\lambda)d\lambda$$
$$+\frac{1}{D_h}\cdot\frac{2D_v^2}{A_v}\cdot\tau_{ml}\cdot\frac{1}{l}\int_0^\infty R(l,\lambda)L_1(z,\lambda)d\lambda$$
$$+\frac{1}{D_h}\cdot\frac{D_v^2}{A_v}\cdot\tau_{m\theta}\int_0^\infty S(l,\lambda)L_1(z,\lambda)d\lambda$$
$$+\frac{1}{D_h}\cdot\frac{D_v^2}{A_v}\cdot\tau_{ml}\int_0^\infty S(l,\lambda)L_2(z,\lambda)\,d\lambda \tag{31}$$

where $S$ is

$$S=J_1(a\lambda)\cdot(J_0(l\lambda)-J_2(l\lambda)). \tag{32}$$

## 2. *Numerical examples*

In the previous paragraph we obtained the expressions for the motion of water induced by a cyclonic storm and we can compute $u$, $v$, $w$ and $\Psi$.

Equation (3) could be considered approximately real wind stress distribution, and it means that $\mathrm{curl}\,\tau>0$ within maximum wind speed point and $\mathrm{curl}\,\tau=0$ outside the point, which acts effectively on upwelling.

To research the main physical characteristics of upwelling, some simple numerical examples are considered.

Let us take the values of $D_v$ as 100 m, $D_h$ as 100 km, respectively, $r_m$ as 100 km, $\phi$ as 30°N and $\tau_m=1$ c.g.s. which corresponds to a wind velocity 5~6 m/s. Also the

Table 1. $\Psi_\theta\times10^5$

| $r/D_h$ | .2 | .4 | .6 | .8 | 1.0 | 1.2 | 1.4 | 1.6 | 1.8 | 2.0 |
|---|---|---|---|---|---|---|---|---|---|---|
| $z/D_v$ | | | | | | | | | | |
| .2 | 66 | −236 | −511 | −842 | −1146 | −1388 | −1433 | −1514 | −1480 | −1454 |
| .4 | −99 | −384 | −824 | −1360 | −1846 | −2239 | −2311 | −2358 | −2349 | −2350 |
| .6 | −114 | −432 | −963 | −1578 | −2139 | −2594 | −2678 | −2715 | −2750 | −2684 |
| .8 | −124 | −487 | −1040 | −1691 | −2275 | −2726 | −2772 | −2766 | −2704 | −2644 |
| 1.0 | −177 | −460 | −991 | −1620 | −2257 | −2700 | −2710 | −2736 | −2711 | −2688 |
| 1.2 | −112 | −453 | −972 | −1573 | −2155 | −2597 | −2678 | −2685 | −2650 | −2614 |
| 1.4 | −111 | −446 | −964 | −1578 | −2134 | −2561 | −2668 | −2643 | −2612 | −2589 |
| 1.6 | −110 | −444 | −958 | −1570 | −2120 | −2553 | −2654 | −2627 | −2597 | −2562 |

Table 2. $K_2 \times 10^4$

| $r/D_h$ | .2 | .4 | .6 | .8 | 1.0 | 1.2 | 1.4 | 1.6 | 1.8 | 2.0 |
|---|---|---|---|---|---|---|---|---|---|---|
| $z/D_v$ | | | | | | | | | | |
| 0 | +142 | +334 | +511 | +696 | +781 | +733 | +519 | +506 | +447 | +398 |
| .2 | +27 | +58 | +98 | +129 | +143 | +125 | +90 | +67 | +50 | +46 |
| .4 | −24 | −45 | −59 | −67 | −74 | −86 | −92 | −84 | −78 | −74 |
| .6 | −29 | −55 | −74 | −91 | −100 | −107 | −100 | −95 | −87 | −79 |
| .8 | −18 | −35 | −48 | −58 | −63 | −66 | −61 | −57 | −51 | −46 |
| 1.0 | −8 | −18 | −22 | −26 | −27 | −28 | −26 | −23 | −21 | −18 |
| 1.2 | −2 | −4 | −6 | −8 | −8 | −6 | −5 | −4 | −3 | −3 |
| 1.4 | 0 | +1 | +1 | +1 | +2 | +2 | +2 | +3 | +3 | +3 |
| 1.6 | +1 | +2 | +2 | +3 | +3 | +3 | +3 | +3 | +3 | +3 |

wind blows tangentially in positive $\theta$ direction. In this case $\Psi_\theta$ are constant in the $r-z$ plane indicating that the projective circulation patterns and the lines of $K_2$ are constant, the vertical variation of $v$ which are the $\theta$ component of the horizontal velocity. Corresponding values of $\Psi_\theta$ and $K_2$ are given in Table 1 and 2.

The value of $\tau_m = 1$ c.g.s. would be necessarily small to explain this phenomena, and $a = 1$ namely $r_m = D_h$ is a rather convenient treatment.

These need research for more precise values. Circulation patterns under these parameters are illustrated in Fig. 3 and 4.

The value of the vertical velocity component $w$ which represents the intensity of the upwelling can be obtained from the function $\Psi$. Table 3 shows the values of $w$ for several $r/D_h$ and $z/D_v$.

From the calculations described above, we may conclude that:

1. After a cyclonic storm has passed, the temperature-depth structures indicate the warm surface water are transported outward from the storm center, and cold water is upwelled along a spiral course from the layer $z = 1.6\ D_v$ or more.
2. The upwelling area is confined to within twice the radius of maximum wind.
3. The warm layers moving outward lead to convergence and downwelling at

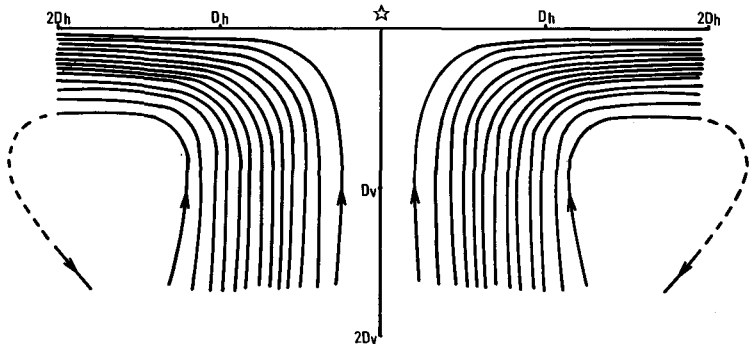


Fig. 3. Upwelling as induced by a circular wind.

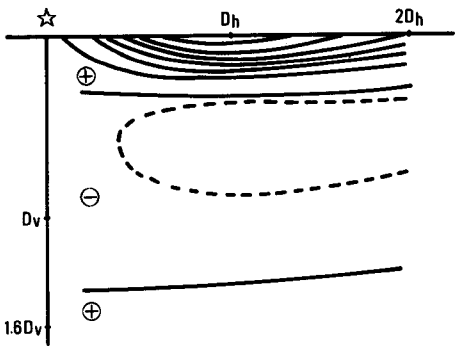


Fig. 4. Vertical distribution of currents v.

Table 3. $w \times 10^3$ cm/sec ($\tau_m = 1$ c.g.s.)

| $r/D_h$ | .2 | .4 | .6 | .8 | 1.0 | 1.2 |
|---|---|---|---|---|---|---|
| $z/D_v$ | | | | | | |
| .2 | −.89 | −1.15 | −1.24 | −1.12 | −.82 | −.62 |
| .4 | −1.34 | −1.92 | −1.98 | −1.81 | −1.31 | −.88 |
| .6 | −1.54 | −2.15 | −2.39 | −2.08 | −1.51 | −1.02 |
| .8 | −1.67 | −2.32 | −2.58 | −2.20 | −1.58 | −1.01 |
| 1.0 | −1.58 | −2.31 | −2.39 | −2.21 | −1.84 | −.74 |
| 1.2 | −1.51 | −2.30 | −2.34 | −2.16 | −1.52 | −.99 |
| 1.4 | −1.51 | −2.24 | −2.39 | −2.10 | −1.50 | −.96 |
| 1.6 | −1.50 | −2.23 | −2.33 | −2.08 | −1.49 | −.97 |

a distance from the center of storm.

4. The maximum upwelling speed can be seen in the center of maximum wind, and its value is about $2.4 \times 10^{-3}$ cm/sec, which corresponds to 2.1 m/day.

5. Under the greatest storm intensity which is approximately regarded as a steady-state condition, a cyclonic current system would be expected in ocean waters around the storm. Current speed is maximum at $r_m$ and it is confined within the surface layer.

## 3. *Case of Hurricane Hilda*

Hurricane Hilda crossed the Gulf of Mexico in the period 30 September to 4 October 1964, developing into a very severe hurricane in the central Gulf.

Two surface water temperature distributions, one based on ships data before the hurricane, and the second on the hydrographic cast after its passage, were measured. Beginning 5 October 1964, a one-week cruise was conducted over the area where hurricane winds had been observed.

The data on all four crossings indicated similar patterns. Temperature-depth structures after the storm indicated that the warm ocean surface layers were driven radially outward from the hurricane center and that cold water upwelled along the hurricane path from a depth of approximately 60 m. The upwelled area extended

100～150 km on each side of the hurricane path. A cyclonic current system was observed in ocean waters around the area of greatest hurricane intensity. The water farthest from the path was characterized by an increase in the depth of the mixed layer.

I) The Gulf of Mexico before hurricane Hilda.

The most useful prior to hurricane Hilda data are sea surface temperature from ships. Some of the Gulf is well travelled by merchant ships and the general character of the sea surface temperature distribution before Hilda was obtained. These data show that from the southeast to the northwest, there was a wide band of

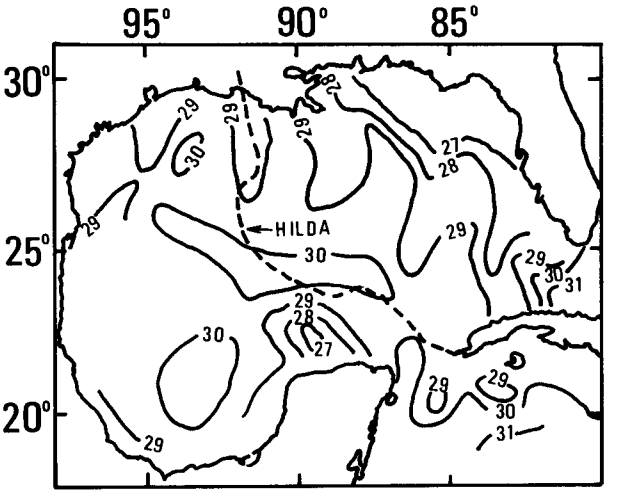


Fig. 5. Sea surface temperature before Hilda, 24-30 Sept., and hurricane path. (after Leipper, 1964, Fig. 1)

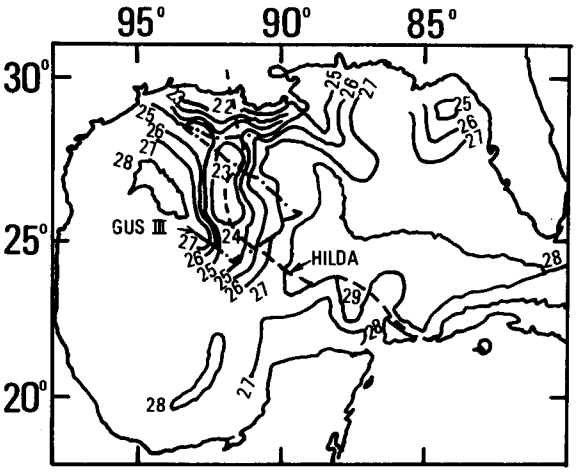


Fig. 6. Sea surface temperature fater Hilda, 1-13 Oct., and hurricane path. (after Leipper, 1964, Fig. 4)

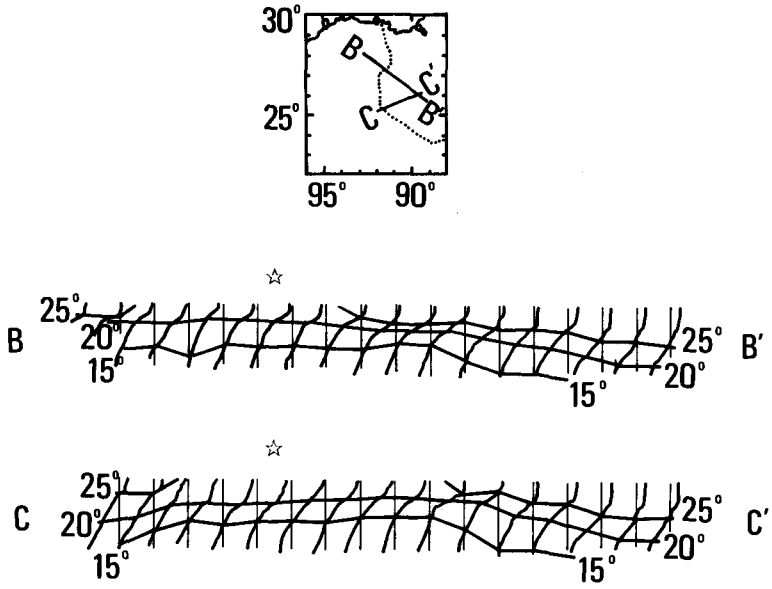


Fig. 7. Copies of BT traces along sections crossing the path of Hilda. (after Leipper, 1964, Fig. 5)

water across the central Gulf having temperatures above 29°C and being fairly uniform at about 29°~30°C (Fig. 5). Other data were obtained from the R/V ALAMINOS which also collected observations before the storm.

II) The Gulf of Mexico after hurricane Hilda

Five marked patterns of sea surface temperatures were found in the Gulf after hurricane Hilda.

a) One feature of sea conditions was that the path of coldest surface water was centered to the west or to the left of the path of the storm (Fig. 6).

This pattern is unexpected, because the effects are less pronounced to the left of eye where forward motion of the hurricane works against the surface wind. The theoretic model assumes symmetry and the above stated coditions can not be explained. It is thought that the colder right side surface water had been carried to the left by the induced cyclonic current.

b) Another marked feature was the vertical sea temperature distribution in different locations with respect to the path of the storm (Fig. 7).

It appeares almost certain that the cold water near the hurricane path rose and the isotherms rose as a result of divergence at the surface and upwelling. These results are in accordance with the theory.

On the other hand, the water farthest from the path was characterized by deep, well mixed surface layers warmer than 25°C. It appears that they had either been mixed by surface cooling, by mechanical action, or both, and that there had been convergence at the surface. The hurricane wind drove well-mixed surface layers radially outward from the center, cooling and mixing it as is moved. The warm layer moving outward led to convergence and downwelling at a distance from the path.

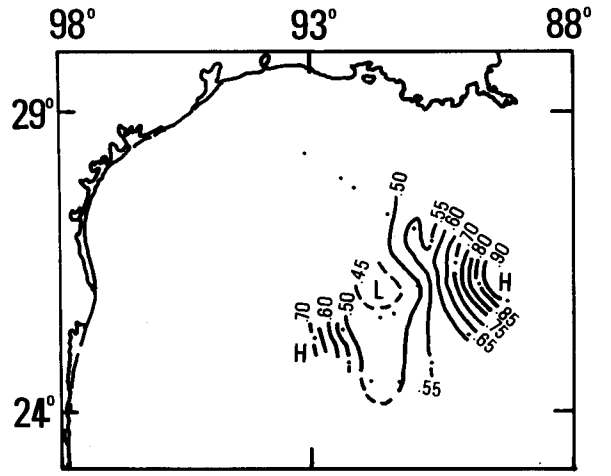


Fig. 8. Dynamic topography of the sea surface referred to 250 db. (after Leipper, 1964, Fig. 7)

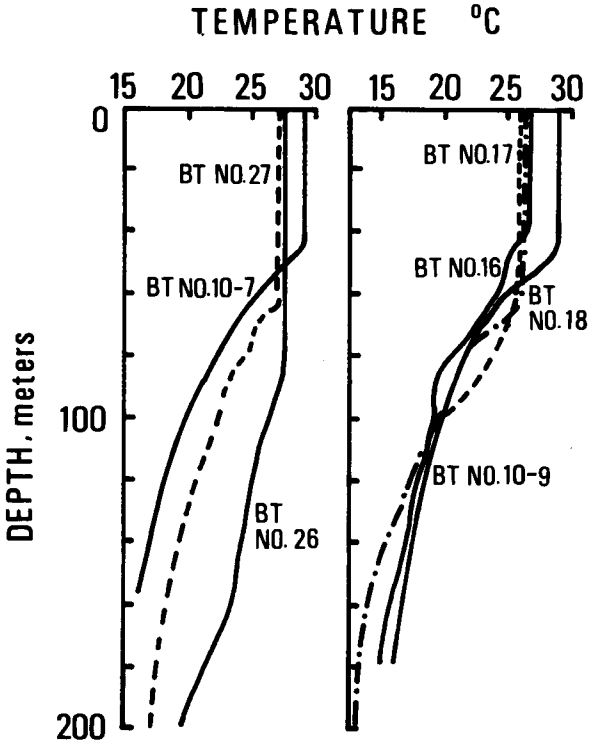


Fig. 9. Comparisons of BTs obtained before and after Hilda at identical locations. (after Leipper, 1964, Fig. 9)

c) A third feature based upon observations made after Hilda is that of the ocean current pattern in the area of the storm. Dynamic topography of the sea surface relative to 250 db was computed by Leipper (1966) (Fig. 8).

The result showed part of a cyclonic current of approximately one knot around the area of coldest water.

Not enough is known about the prevailing current in this area in summer to ascertain whether or not the current was set up by the hurricane.

However it is clear that any such prevailing current would have been intensified in the presence of the cold upwelled water.

d) A fourth feature is the depth of upwelling. Comparison of BTs obtained before and after Hilda are shown in Fig. 9. Cold surface waters must have come from depths of the order 60 m, considering the temperature-depth structure which is normal in this part of the Gulf in summer.

This upwelling depth is shallower than the theoretical value, but it is thought that the frictional depth in this area is shallow.

e) The fifth feature is the area of upwelling. Sea surface temperatures decreased by more than 5°C over an area of some 40 to 100 km, and the upwelled area extended 100~150 km on each side of this path. This was in accordance with the theory.

*4. Case of typhoon Shirly*

From 2 to 5 September 1965, the R/V Atlantis II made an oceanographic section across Kuroshio, south of Shikoku, Japan. On 9 September Typhoon Shirly passed across Japan. Shirly was in its most intense stage when it crossed the Kuroshio area.

The ship returned to the sea on 10 September and observations were made again. Two temperature sections across the track of Shirly in the vicinity of the

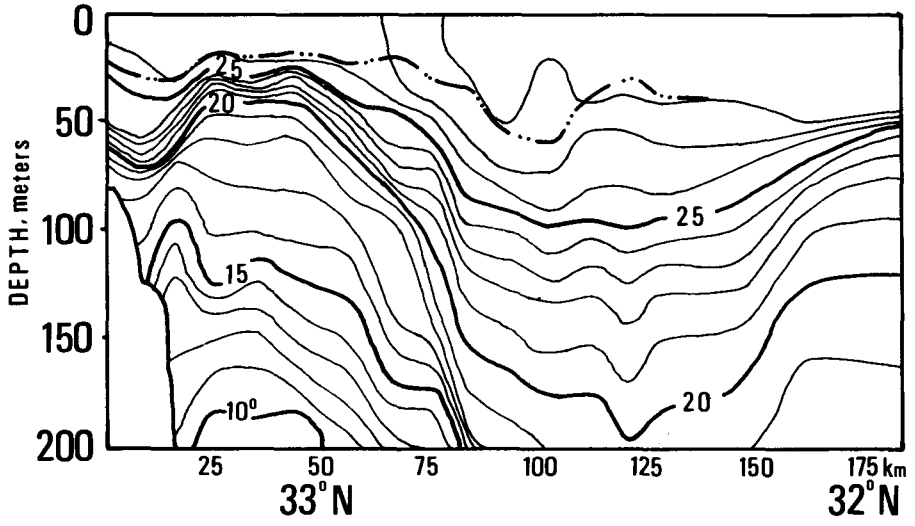


Fig. 10. Temperature section before Typhoon Shirley. (after Wright, 1968, Fig. 2)

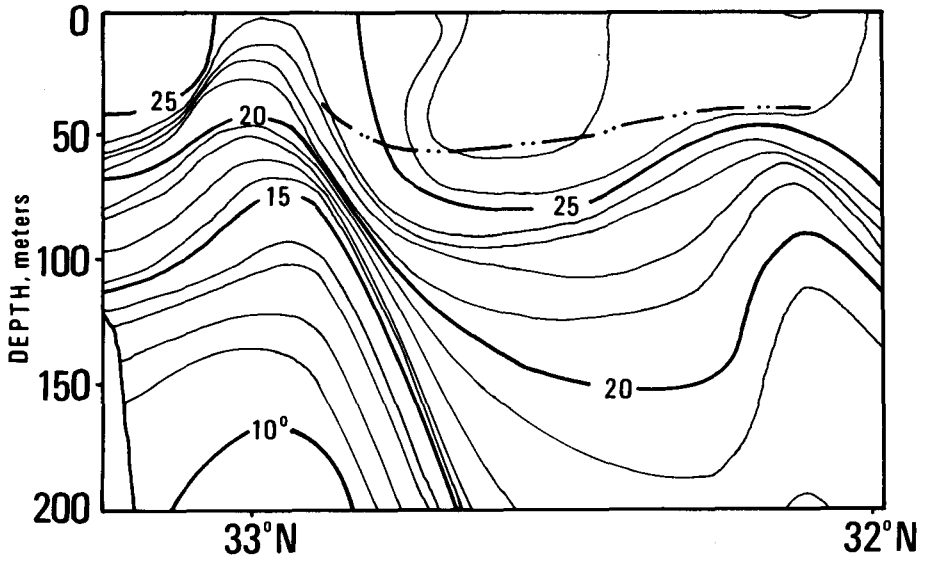


Fig. 11. Temperature section after Typhoon Shirley. (after Wright, 1968, Fig. 3)

Kuroshio were produced (Fig. 10 and 11).

a) The most striking change occured under the eye, where the isotherms were raised. Cold water had risen from below to replace the surface layer, and there was a 3°C drop in surface water temperature.

b) To the south of the storm the effect was greater, as shown by both upward displacement of the isotherm and a decrease in surface water temperature of one or two degrees. The 28°C isotherms disappeared and the 27°C isotherms were found only in a few places. The 20°C and 25°C isotherms rose from 25 to 30 m, and both the 10°C and 15°C isotherms were appreciably shallower after the storm.

Little of the above described effects were noted on the inshore side, as the storm passed near land.

It was also noted in this case that the effects were less pronounced to the left of the eye, where foward motion of the storm works against the surface wind. The deeping of the mixed layer, where it was clearly defined, was greater to the right of the eye.

These results are in accordance with the theory which requires upwelling under the eye of a cyclonic storm to replace the surface water that is driven radially outward. The upwelling continued for more than a day after the storm passed.

c) Although the large temperature changes which probably occurred in the surface water directly under the eye could not be observed. The greatest change under the eye occurred in deeper water from 80 to 170 m. At a depth of about 60 m the temperature changed very little.

The upwelling area was confined within twice the radius of maximum wind in both storms observed.

BT and Nansen bottle traces before and after the storm (Fig. 12) indicate that cold water had come from 200 m which is coincident with the theory.

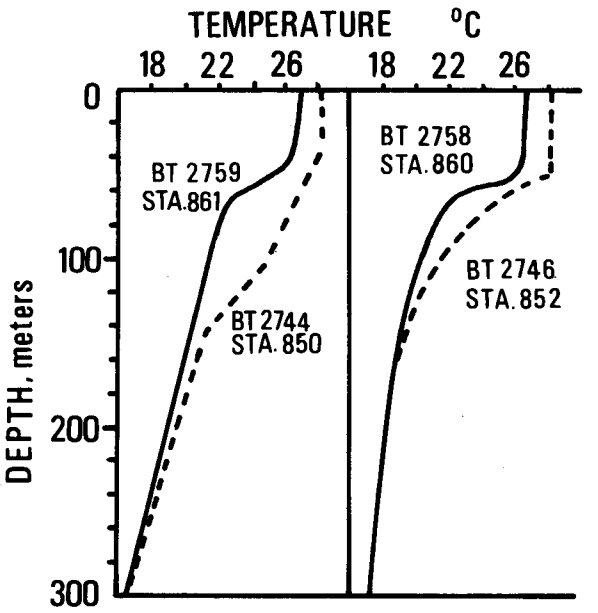


Fig. 12. Comparison of pairs of BTs and Nansen bottle observation made before and after the storm. (after Wright, 1968, Fig. 5)

d) Wright (1969) calculated upwelling speed in a moderate typhoon according to the theory and the calculated value 13 m per day was determined in Shirly. The speed with which isotherms raised showed this value.

But steady-state model could not explain transient process, and upwelling speed is a weak point in a steady-state model.

## Summary

An attempt has been made to compare a steady-state upwelling theory with oceanographic observations following two storms, Hilda and Shirly.

The theory explains well that within a cyclonic circular wind system, intense upwelling occurres within the area twice the radius of maximum wind, water upwells from under the frictional depth generated by the cyclonic current system. But this steady-state model cannot explain upwelling speed sufficiently.

## References

Hidaka, K. 1954. A contribution to the theory of upwelling and coastal currents. *T.A.G.U.* **35**(3), 431-444.

Hidaka, K. and Akiba, Y. 1955. Upwelling induced by a circular wind system. *Records Ocean. Works Japan 2*, 7-18.

Leipper, D.F. 1966. Observed ocean conditions and hurricane Hilda, 1964. *J. Atmos. Sci.*, **24**, 182-196.

Wright, R. 1969. Temperature structure across the Kuroshio before and after typhoon Shirly. *Tellus XXI* **3**, 409-413.